



NON-LINEAR DYNAMICS OF A SUSPENDED TRAVELLING CABLE SUBJECT TO TRANSVERSE FLUID EXCITATION

H. Y. HU AND D. P. JIN

*Institute of Vibration Engineering Research, Nanjing University of Aeronautics and Astronautics,
210016 Nanjing, People's Republic of China. E-mail: hhyae@nuaa.edu.cn*

(Received 23 March 2000, and in final form 20 June 2000)

Starting with the analysis of the fluid drag and lift on a suspended travelling cable subjected to transverse fluid excitation, the paper presents the expression of forces on the cable, and then a set of partial differential equations of in-plane and out-of-plane motions of the cable. In the case of small ratio of sag to span, the in-plane and out-of-plane modes of the first order dominate the motions of cable. Thus, the partial differential equations of cable are reduced to two ordinary differential equations of the second order by means of the Galerkin approach. Because the stiffness terms disappear in the ordinary differential equations when the cable is at equilibrium position, the co-ordinate transform proposed by Pilipchuk is used to describe the stretch and rotation of mid-span section of cable from the equilibrium position so that the transformed differential equations include linear stiffness terms. Afterwards, the differential equations are simplified by using the perturbation approach of two variables under the assumption that the Young's module of cable is not very small. As a result, the approximate cable dynamics yields a two-dimensional autonomous system and does not exhibit any chaotic motions. According to the approximated model, two equilibrium positions of cable are determined and their stability is analyzed. Finally, the influences of travelling velocity and cable density on the cable dynamics are discussed on the basis of numerical computations. The case studies show that the travelling velocity should be limited when a very light cable is laid under water in order to avoid harmful and dangerous swings.

© 2001 Academic Press

1. INTRODUCTION

Suspended travelling cables are extensively used in various fields of engineering. The observed cable dynamics often exhibits complex non-linear behavior. Here are a few, but typical examples. (1) The cable of shipping crane may have aperiodic swings and produce poor position accuracy. (2) The balloon formation in ring spinning process often limits the moving speed of the yarn. (3) The tethered satellite deployed from an orbiting shuttle may undergo very complex vibration. Hence, it is essential to understand and predict the complicated non-linear dynamics of suspended travelling cables in their design phase.

In marine engineering, the dynamics of underwater cables, as an important topic, has drawn much attention since 1970s. For example, Choo and Casarella reviewed the early work on the mathematical models for anchoring cables with hydrodynamics taken into account [1]. Nair and Hung analyzed the stability of a towing cable immersed in water [2, 3]. Papazoglou and his co-authors made an experiment on the non-linear response of a cable immersed in water [4]. Recently, Vassalos and Huang summarized four types of analysis methods for the marine cable dynamics and presented the numerical simulation and experiment of a marine cable, one of ends of which is subjected to horizontal excitation

[5]. Mavrakos and Chatjigeorgiou studied the dynamic behavior of mooring cable with submerged buoys [6]. They found a way to reduce the dynamic tension of the cable by properly choosing buoys and their positions. Chang and his co-authors presented a detailed analysis of non-linear interaction of the first two in-plane modes of a suspended cable subjected to a fluid flow in direction of cable [7]. To the authors' knowledge, however, the non-linear dynamics of suspended travelling cables subject to transverse fluid flow is still an open problem.

When an underwater cable is being laid, it is travelling at certain velocity. This makes the cable dynamics are complicated than a suspended cable. Intensive studies have been made for the dynamics of travelling cable in air, such as the deployed cable of a tethered satellite, tapes of video recorder. For example, Pekins and Mote Jr. established the three-dimensional non-linear dynamic model for an arbitrarily sagged travelling cable with arbitrarily inclined eyelets in air by using the description of finite strain [8]. Compared with those studies, the dynamics of underwater cable is a tougher problem.

The aim of this paper is to reveal the dynamics of a suspended travelling cable under the transverse fluid flow. The paper is organized as follows. To properly describe the cable dynamics, the fluid drag and the lift on the cable are analyzed first. Then a set of partial differential equations of motion is established. The Galerkin approach, the Pilipchuk transform and the perturbation technique of two variables are successively used to simplify the partial differential equations to a two-dimensional autonomous system. Afterwards, the equilibrium positions and their stability are analyzed in detail. Finally, some case studies are discussed.

2. MODEL OF A SUSPENDED TRAVELLING CABLE

As shown in Figure 1, a cable, subjected to a transverse, uniformly distributed fluid flow at constant velocity V_f , is moving at constant velocity c through two eyelets spanned under water. The dashed curve in Figure 1 represents the static configuration of cable in still water. To describe the motion of cable, a set of Cartesian co-ordinates is established in Figure 1 such that the x -axis connects the two eyelets, the y -axis is on the horizontal plane and perpendicular to x -axis, and the z -axis points the direction of gravity. In addition, an arc co-ordinate s is introduced along the cable to position the specific section of the cable.

In the frame of Cartesian co-ordinates, the fluid flow moves in the y direction and drives an arbitrary inertial point of the travelling cable from the spatial position $P^i(x, v_0, w_0)$ to $P^f(x + u, v, w)$ as shown in Figure 1. The accurate modelling of a cable gives rise to a non-linear dynamic system having infinite degrees of freedom. In the case of small ratio of

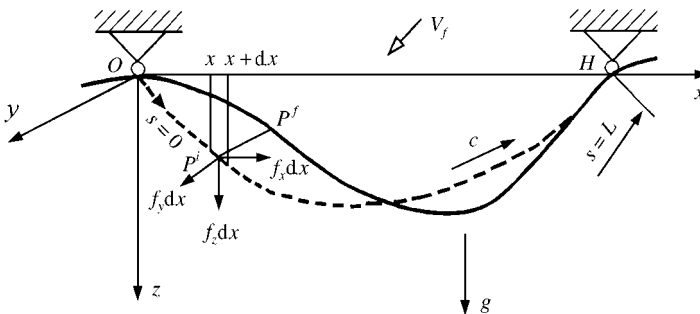


Figure 1. A suspended travelling cable subjected to transverse fluid flow.

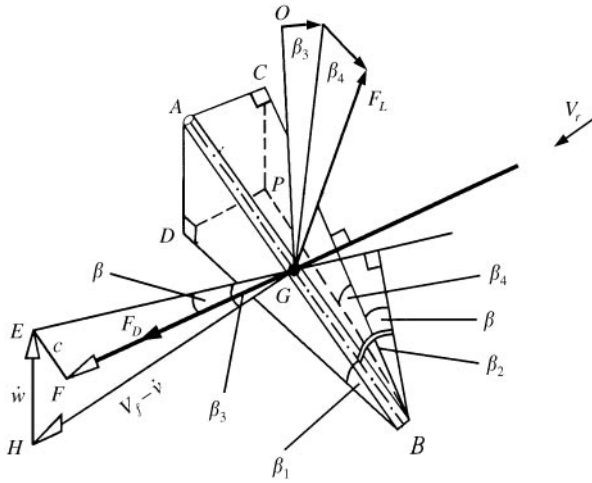


Figure 2. The forces on a short segment of travelling cable.

sag-to-span, say 1 : 8, it has been proved that such a complicated system could be greatly simplified. In this paper, the small sag-to-span ratio is a basic assumption. Hence, the slope and curvature of the cable are also very small.

To analyze the forces applied on the cable, a short segment AB of length ds is separated from the cable and shown in Figure 2. In the frame of Cartesian co-ordinates, the external force on the cable segment can be decomposed as f_x , f_y and f_z . The forces on the cable element AB are shown in Figure 2. As the cable is moving at velocity c , the segments EF and AB are parallel to each other. From the vector relation $\mathbf{V}_r = \dot{\mathbf{u}} + \dot{\mathbf{w}} + (\mathbf{V}_f - \dot{\mathbf{v}})$, the relative velocity of fluid flow to cable is in the direction GF and has magnitude V_r , where the dot represents the partial derivative with respect to time t . In the case of small sag-to-span ratio, the angle between the segment AB and the horizontal plane xoy is $\beta_1 \approx w' \ll 1$, and the angle between the segment AB and the vertical plane xoz is $\beta_2 \approx v' \ll 1$, where the prime represents the partial derivative with respect to the co-ordinate x .

Let F_D be the fluid drag, along the segment GF , on the cable segment AB . It is obvious that the fluid lift F_L is perpendicular to the plane spanned by the segment GF and the cable segment AB . Let the segment OG rotate an angle β_3 in the plane EGH , and then rotate an angle β_4 around the force vector F_D . Thus, the direction of fluid lift F_L can be determined. According to the Morison drag term in hydrodynamics, it is easy to write out the fluid drag and lift on the cable element of unit length

$$F_D = \frac{1}{2} \rho_f D_C C_D V_r |V_r|, \quad F_L = \frac{1}{2} \rho_f D_C C_L V_r |V_r|, \quad (1)$$

where ρ_f is the fluid density, D_C the equivalent diameter of cable section, C_D and C_L are the coefficients of fluid drag and lift respectively. In the frame of Cartesian co-ordinates defined above the contributions of fluid drag and lift are expressed as

$$f_y = F_D \cos \beta \cos \beta_3 - F_L \cos \beta_4 \sin \beta_3, \quad f_z = -F_D \cos \beta \sin \beta_3 - F_L \cos \beta_4 \cos \beta_3. \quad (2)$$

In what follows, it is assumed that the flow velocity V_f is much larger than the velocity components of cable in directions y and z , i.e., $\dot{v}/V_f \ll 1$ and $\dot{w}/V_f \ll 1$. From the triangle EFG in Figure 2 and the cosine theorem, one can derive the relative velocity between the cable and flow

$$V_r \approx b V_f (1 - \bar{k}v'), \quad (3)$$

where

$$b = \sqrt{1 + \lambda_0^2}, \quad \bar{k} = \frac{\lambda_0}{1 + \lambda_0^2}, \quad \lambda_0 = \frac{c}{V_f}. \quad (4)$$

By substituting the following geometric relations:

$$\cos \beta = \frac{(1 - \lambda_0 v')V_f}{V_r}, \quad \cos \beta_3 = \frac{V_f - \dot{v}}{V_f}, \quad \sin \beta_3 = \frac{\dot{w}}{V_f}, \quad \cos \beta_4 \approx 1 \quad (5)$$

into equation (2), one obtains the components of fluid force on the cable element of unit length

$$\begin{aligned} f_y &= -\frac{1}{2} \rho_f b D_C V_f [b C_L \dot{w}(1 - \bar{k}v') - C_D(V_f - \dot{v})(1 - \lambda_0 v')](1 - \bar{k}v'), \\ f_z &= -\frac{1}{2} \rho_f b D_C V_f [b C_L(V_f - \dot{v})(1 - \bar{k}v') + C_D \dot{w}(1 - \lambda_0 v')](1 - \bar{k}v'). \end{aligned} \quad (6)$$

According to the Hamilton principle, one can derive a set of partial equations that govern the dynamics of suspended travelling cable as follows:

$$\frac{\partial^2 v}{\partial t^2} - \frac{\partial^2 v}{\partial s^2} \frac{E}{\rho} \bar{\varepsilon} = \frac{f_y}{\rho A}, \quad \frac{\partial^2 w}{\partial t^2} - \frac{\partial^2 w}{\partial s^2} \frac{E}{\rho} \bar{\varepsilon} = \frac{f_z}{\rho A} + \bar{g}, \quad (7)$$

where

$$\rho = \rho_c + C_I \rho_f, \quad \bar{g} = \frac{g \rho_c}{\rho}, \quad (8)$$

ρ_c is the density of the cable, C_I the coefficient of fluid inertial attached to the cable, g the gravitational acceleration, A the section area of cable, E the Young's module of cable, and $\bar{\varepsilon}$ the averaged longitudinal stain of cable as defined in reference [7]:

$$\bar{\varepsilon}(t) = \frac{1}{2H} \int_0^H \left[\left(\frac{\partial v}{\partial x} \right)^2 + \left(\frac{\partial w}{\partial x} \right)^2 - \left(\frac{\partial w_0}{\partial x} \right)^2 \right] dx. \quad (9)$$

Here $w_0(x) = D \sin(\pi x/H)$ is the static configuration of the cable at the equilibrium position in still water, H the span of cable, and D the sag of cable in the absence of gravity.

3. SYSTEM REDUCTION AND PILIPCHUK TRANSFORM

To simplify the dynamic equation (7) with the expressions of fluid force substituted, a set of new variables and parameters are defined first

$$\begin{aligned} \eta = \frac{x}{H}, \quad V = \frac{v}{D}, \quad W = \frac{w}{D}, \quad \tau = \frac{d}{H} \sqrt{\frac{E}{\rho}} t, \quad d = \frac{D}{H}, \quad \mu = \sqrt{\frac{\rho_c g H^4}{E D^3}}, \\ c_f = \frac{C_L}{C_D}, \quad v_f = \frac{V_f}{d^2} \sqrt{\frac{\rho}{E}}, \quad D_f = \frac{b \rho_f v_f C_D D_C D}{2 \rho A}, \quad \lambda = d \lambda_0, \quad k = d \bar{k}. \end{aligned} \quad (10)$$

Then, the in-plane and out-of-plane motions of cable are approximated by the vibration modes of the first order as follows:

$$V(\eta, \tau) = \sin(\pi \eta) q_1(\tau), \quad W(\eta, \tau) = \sin(\pi \eta) q_2(\tau). \quad (11)$$

By means of the Galerkin approach, equation (7), with equation (6) substituted, is simplified as

$$\begin{aligned} \ddot{q}_1 + \varepsilon_q q_1 &= -D_f \{ m\dot{q}_2 + \dot{q}_1 - \delta_1 v_f + \sigma q_1^2 [m\dot{q}_2 + n(\dot{q}_1 - \delta_2 v_f)] \}, \\ \ddot{q}_2 + \varepsilon_q q_2 &= -D_f \{ \dot{q}_2 - m(\dot{q}_1 - \delta_1 v_f) + \sigma q_1^2 [n\dot{q}_2 - m(\dot{q}_1 - \delta_2 v_f)] \} + \delta_1 \mu^2, \end{aligned} \tag{12}$$

where

$$\varepsilon_q = \frac{\bar{\varepsilon}}{d^2} = \frac{\pi^2}{4} (q_1^2 + q_2^2 - 1), \quad \sigma = \frac{k^2 \pi^2}{4}, \quad m = bc_f, \quad n = 1 + \lambda_0^2, \quad \delta_1 = \frac{4}{\pi}, \quad \delta_2 = \frac{16}{3\pi}. \tag{13}$$

The dot in equation (12) is redefined as the derivative with respect to the dimensionless time τ . This equation governs the horizontal and vertical motions of the mid-span section of cable.

Intuitively speaking, the motion of mid-span section of cable is similar to that of a spring pendulum of two degrees of freedom. Like the study on the spring pendulum, it is very natural to consider a co-ordinate transform suggested by Pilipchuk in reference [9]:

$$q_1(\tau) = [1 + \zeta(\tau)] \sin \varphi(\tau), \quad q_2(\tau) = [1 + \zeta(\tau)] \cos \varphi(\tau), \tag{14}$$

where $\zeta(\tau)$ and $\varphi(\tau)$ are the radial stretch and the rotation angle of mid-span section of cable respectively. As shown in Figure 3, φ is measured from the bottom position of cable, where the cable is at rest in still water, and in clockwise direction.

From equation (14), one can see that $\zeta = 0$ corresponds to the circular motion of mid-span section of cable. For this kind of motion, one has

$$\varepsilon_q = \frac{\pi^2}{4} (q_1^2 + q_2^2 - 1) = 0. \tag{15}$$

Equation (15) indicates that the averaged longitudinal strain of cable vanishes when the mid-span section of cable moves exactly on the unit circle. So do all the stiffness terms in equation (12). This phenomenon usually makes a trouble to the perturbation analysis. One can immediately find, however, that in the new co-ordinates, at least one dynamic equation remains a stiffness term.

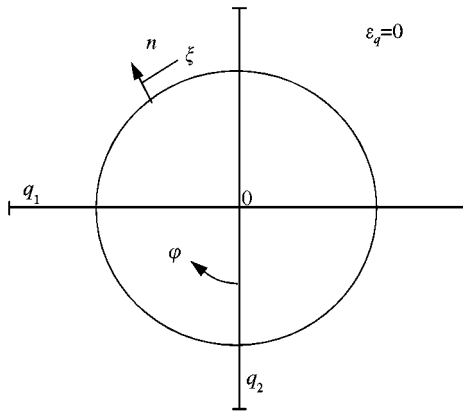


Figure 3. Definition of new variables in Pilipchuk transform.

By substituting transform (14) into Equation (12) and neglecting the higher order terms of ξ , one obtains a set of dynamic equations that govern the stretch and rotation of mid-span section of cable as following:

$$\ddot{\xi} + D_f \dot{\xi} + \omega_0^2 \xi - (mD_f - \dot{\varphi})\dot{\varphi} - \frac{dF(\varphi)}{d\varphi} + G(\dot{\xi}, \varphi, \dot{\varphi}) \sin^2 \varphi = 0, \quad (16a)$$

$$\ddot{\varphi} + D_f \dot{\varphi} + (mD_f + 2\dot{\varphi})\dot{\xi} + F(\varphi) + H(\dot{\xi}, \varphi, \dot{\varphi}) \sin^2 \varphi = 0, \quad (16b)$$

where

$$\begin{aligned} F(\varphi) &= \delta_1[(\mu^2 - mD_f v_f) \sin \varphi - D_f v_f \cos \varphi], \\ G(\dot{\xi}, \varphi, \dot{\varphi}) &= \sigma_1(n\dot{\xi} - m\dot{\varphi}) - 4\sigma_2(n \sin \varphi - m \cos \varphi), \\ H(\dot{\xi}, \varphi, \dot{\varphi}) &= \sigma_1(m\dot{\xi} + n\dot{\varphi}) - 4\sigma_2(m \sin \varphi + n \cos \varphi) \end{aligned} \quad (17)$$

and

$$\omega_0 = \frac{\pi^2}{\sqrt{2}}, \quad \sigma_1 = \frac{\pi^2 k^2 D_f}{4}, \quad \sigma_2 = \frac{\pi k^2 D_f v_f}{3}. \quad (18)$$

Now, the elastic restoring force in cable gives rise to the static stiffness terms in equation (16a) as long as the motion of mid-span section of cable deviates from the unit circle. Even if the mid-span section of cable is moving along the unit circle, the effects of gravity, fluid drag and lift still offer a stiffness term to equation (16b).

4. APPROXIMATE SOLUTION

To further simplify equation (16), an important phenomenon of cable dynamics should be noticed. That is, the magnitude of radial stretch of mid-span section of cable is usually much smaller than the magnitude of rotation angle since the Young's module of a real cable cannot be very small. This is the case when the cable is made of metal or even glass fibre. In most cases, the assumption of $E \gg \rho_c g H^4 / D^3$ holds true, there follows a small parameter μ according to its definition in equation (10). When a steel cable under water is taken as an example, the curves of small μ versus H for some practical ratios of sag-to-span are shown in Figure 4.

In the case of small μ , the perturbation technique can be used to give an approximate analysis of cable dynamics under the transverse fluid flow. For this purpose, one can rescale the time, generalized displacements and two parameters as follows:

$$t_0 = \mu\tau, \quad \xi = \mu^2 \bar{\xi}(\tau), \quad \varphi = \hat{\varphi}(\mu\tau) + \mu^2 \bar{\varphi}(\tau), \quad D_f = \mu \bar{D}_f, \quad v_f = \mu \bar{v}_f. \quad (19)$$

By substituting equation (19) into equation (16) and dropping the higher order terms, one obtains

$$\begin{aligned} \ddot{\bar{\xi}} + \omega_0^2 \bar{\xi} &= -\left(\frac{d\hat{\varphi}}{dt_0}\right)^2 + 2\mu\dot{\hat{\varphi}} \frac{d\hat{\varphi}}{dt_0} + \bar{Q}_1 \left(\frac{d\hat{\varphi}}{dt_0} + \mu\dot{\hat{\varphi}}\right) - \bar{Q}_2 \mu \dot{\bar{\xi}} + \bar{Q}_3 \sin \hat{\varphi} + \bar{Q}_4 \cos \hat{\varphi}, \\ \ddot{\hat{\varphi}} &= -\frac{d^2 \hat{\varphi}}{dt_0^2} - 2\mu \dot{\bar{\xi}} \frac{d\hat{\varphi}}{dt_0} - \bar{Q}_2 \left(\frac{d\hat{\varphi}}{dt_0} + \mu\dot{\hat{\varphi}}\right) - \bar{Q}_1 \mu \dot{\bar{\xi}} - \bar{Q}_4 \sin \hat{\varphi} + \bar{Q}_3 \cos \hat{\varphi}, \end{aligned} \quad (20)$$

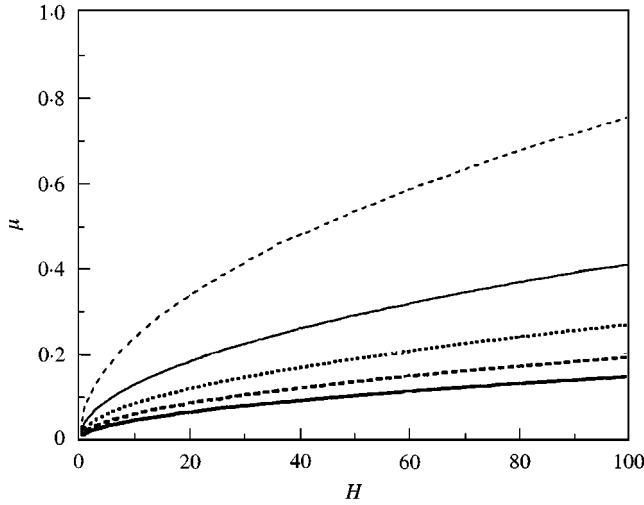


Figure 4. Small parameter μ versus span H at practical ratios of sag-to-span ($g = 9.8 \text{ m/s}^2$, $\rho_c = 7.8 \times 10^3 \text{ kg/m}^3$, $E = 210 \text{ GPa}$). —, $d = 0.12$; ----, $d = 0.10$; ·····, $d = 0.08$; — · —, $d = 0.06$; - - - - - , $d = 0.04$.

where

$$\bar{\sigma}_1 = \frac{k^2 \pi^2 \bar{D}_f}{4}, \quad \bar{\sigma}_2 = \frac{k^2 \pi \bar{D}_f \bar{v}_f}{3},$$

$$\bar{Q}_1 = m(\bar{D}_f + \bar{\sigma}_1 \sin^2 \hat{\phi}), \quad \bar{Q}_2 = \bar{D}_f + n\bar{\sigma}_1 \sin^2 \hat{\phi}, \tag{21}$$

$$\bar{Q}_3 = \delta_1(\bar{D}_f \bar{v}_f + \pi n \bar{\sigma}_2 \sin^2 \hat{\phi}), \quad \bar{Q}_4 = \delta_1[1 - m(\bar{D}_f \bar{v}_f + \pi \bar{\sigma}_2 \sin^2 \hat{\phi})].$$

Let $\tilde{t} = \omega_0 \tau$ be a new dimensionless time scale, i.e., $\bar{\xi} = \bar{\xi}(\tilde{t}, t_0)$ and $\bar{\varphi} = \bar{\varphi}(\tilde{t}, t_0)$. It is easy to see that equation (20) involves a slow time scale t_0 and a fast time scale \tilde{t} . According to the two variable perturbation approach [10], the solution of equation (20) should be in the form

$$\bar{\xi} = \bar{\xi}_0(\tilde{t}, t_0) + \mu \bar{\xi}_1(\tilde{t}, t_0) + O(\mu^2), \tag{22}$$

$$\bar{\varphi} = \bar{\varphi}_0(\tilde{t}, t_0) + \mu \bar{\varphi}_1(\tilde{t}, t_0) + O(\mu^2).$$

By substituting equation (22) into equation (20) and equating the same power of μ , one has

$$\omega_0^2 \left(\frac{\partial^2 \bar{\xi}_0}{\partial \tilde{t}^2} + \bar{\xi}_0 \right) = - \left(\frac{d\hat{\phi}}{dt_0} \right)^2 + \bar{Q}_1 \frac{d\hat{\phi}}{dt_0} + \bar{Q}_3 \sin \hat{\phi} + \bar{Q}_4 \cos \hat{\phi}, \tag{23}$$

$$\omega_0^2 \frac{\partial^2 \bar{\varphi}_0}{\partial \tilde{t}^2} = - \frac{d^2 \hat{\phi}}{dt_0^2} - \bar{Q}_2 \frac{d\hat{\phi}}{dt_0} - \bar{Q}_4 \sin \hat{\phi} + \bar{Q}_3 \cos \hat{\phi}, \tag{24}$$

$$\omega_0^2 \left(\frac{\partial^2 \bar{\xi}_1}{\partial \tilde{t}^2} + \bar{\xi}_1 \right) = 2\omega_0 \left(\frac{d\hat{\phi}}{dt_0} \frac{\partial \bar{\varphi}_0}{\partial \tilde{t}} - \frac{\partial^2 \bar{\xi}_0}{\partial \tilde{t} \partial t_0} \right) + \omega_0 \left(\bar{Q}_1 \frac{\partial \bar{\varphi}_0}{\partial \tilde{t}} - \bar{Q}_2 \frac{\partial \bar{\xi}_0}{\partial \tilde{t}} \right), \tag{25}$$

$$\omega_0^2 \frac{\partial^2 \bar{\varphi}_1}{\partial \tilde{t}^2} = - 2\omega_0 \frac{d\hat{\phi}}{dt_0} \frac{\partial \bar{\xi}_0}{\partial \tilde{t}} - \omega_0 \left(\bar{Q}_2 \frac{\partial \bar{\varphi}_0}{\partial \tilde{t}} + \bar{Q}_1 \frac{\partial \bar{\xi}_0}{\partial \tilde{t}} \right). \tag{26}$$

Because the right-hand side of equation (23) involves the slow time scale t_0 only, the solution of equation (23) reads

$$\bar{\xi}_0 = A_0(t_0) \sin(\tilde{t}) + B_0(t_0) \cos(\tilde{t}) + \frac{1}{\omega_0^2} \left[-\left(\frac{d\hat{\phi}}{dt_0}\right)^2 + \bar{Q}_1 \frac{d\hat{\phi}}{dt_0} + \bar{Q}_3 \sin \hat{\phi} + \bar{Q}_4 \cos \hat{\phi} \right], \tag{27}$$

where $A_0(t_0)$ and $B_0(t_0)$ are the functions in slow time scale. Similarly, solving equation (24) for $\bar{\varphi}_0$ and dropping the secular terms give

$$\bar{\varphi}_0 = 0. \tag{28}$$

From the cancellation condition of secular terms in equations (25) and (26), one can find the approximate solution of the first order for equation (16):

$$\xi = \mu^2(\alpha_0 \sin \omega_0\tau + \beta_0 \cos \omega_0\tau)e^{-Q_2\tau} + \frac{1}{\omega_0^2} \left[-\left(\frac{d\hat{\phi}}{d\tau}\right)^2 + Q_1 \frac{d\hat{\phi}}{d\tau} + Q_3 \sin \hat{\phi} + Q_4 \cos \hat{\phi} \right], \tag{29}$$

$$\varphi = \hat{\phi} + \frac{\mu^2}{\omega_0} \left(2 \frac{d\hat{\phi}}{d\tau} + Q_1 \right) (\alpha_0 \cos \omega_0\tau - \beta_0 \sin \omega_0\tau) e^{-Q_2\tau},$$

where α_0 and β_0 are the arbitrary parameters determined by the initial conditions, whereas

$$\begin{aligned} Q_1 &= mD_f + \sigma_1 \sin^2 \hat{\phi}, & Q_2 &= D_f + n\sigma_1 \sin^2 \hat{\phi}, \\ Q_3 &= \delta_1(D_f v_f + \pi n\sigma_2 \sin^2 \hat{\phi}), & Q_4 &= \delta_1[\mu^2 - m(D_f v_f + \pi\sigma_2 \sin^2 \hat{\phi})]. \end{aligned} \tag{30}$$

From equations (24) and (28), one can see that $\hat{\phi}$ yields

$$\frac{d^2 \hat{\phi}}{d\tau^2} + Q_2 \frac{d\hat{\phi}}{d\tau} + Q_4 \sin \hat{\phi} - Q_3 \cos \hat{\phi} = 0. \tag{31}$$

In the sense of the first order approximation, equation (31) serves as a simplified dynamic equation of the original cable system. As equation (31) is equivalent to a two-dimensional autonomous system, the approximated model of cable does not exhibit any chaotic motions. Furthermore, Q_2 , the coefficient of velocity term, involves the parameter $D_f > 0$ and keeps positive. Hence, the system is energy dissipative and does not undergo any Hopf bifurcation.

5. STABILITY ANALYSIS OF EQUILIBRIUM POSITIONS

5.1. DETERMINATION OF EQUILIBRIUM POSITIONS

From equation (16), the equilibrium position (φ_0, ξ_0) yields

$$\omega_0^2 \xi_0 - \frac{dF(\varphi_0)}{d\varphi_0} + G(0, \varphi_0, 0) \sin^2 \varphi_0 = 0, \quad F(\varphi_0) + H(0, \varphi_0, 0) \sin^2 \varphi_0 = 0, \tag{32a,b}$$

namely

$$\xi_0 = \frac{1}{\omega_0^2} \left[\frac{dF(\varphi_0)}{d\varphi_0} + 4\sigma_2(n \sin \varphi_0 - m \cos \varphi_0) \sin^2 \varphi_0 \right], \tag{33a}$$

$$F(\varphi_0) - 4\sigma_2(m \sin \varphi_0 + n \cos \varphi_0) \sin^2 \varphi_0 = 0. \tag{33b}$$

One can first solve equation (33b) for the rotation angle φ_0 and then gets the radial stretch ξ_0 from equation (33a).

For simplicity, first consider the case when the cable is not travelling in direction x , i.e., $c = 0$. This results in

$$\lambda_0 = 0, \quad m = c_f, \quad n = 1, \quad \sigma_2 = 0 \quad (34)$$

such that equation (33) is simplified as

$$\xi_0 = \frac{1}{\omega_0^2} \frac{dF(\varphi_0)}{d\varphi_0} = \frac{8}{\pi^5} [(\mu^2 - c_f v_f D_f) \cos \varphi_0 + v_f D_f \sin \varphi_0] \quad (35a)$$

$$F(\varphi_0) = \delta_1 [(\mu^2 - c_f v_f D_f) \sin \varphi_0 - v_f D_f \cos \varphi_0] = 0. \quad (35b)$$

Solving equation (35b) for φ_0 gives two possible angles of equilibrium

$$\varphi_{01} = \arccos \frac{\mu^2 - c_f v_f D_f}{\sqrt{(\mu^2 - c_f v_f D_f)^2 + (v_f D_f)^2}} \in (0, \pi), \quad \varphi_{02} = \varphi_{01} + \pi \in (\pi, 2\pi). \quad (36)$$

The corresponding values of radial stretch are

$$\xi_{01,2} = \pm \frac{8}{\pi^5} \sqrt{(\mu^2 - c_f v_f D_f)^2 + (v_f D_f)^2}. \quad (37)$$

According to Figure 3, the equilibrium positions corresponding to (φ_{01}, ξ_{01}) and (φ_{02}, ξ_{02}) are referred to as the left equilibrium position and the right equilibrium position respectively.

In the case of $\mu^2 > c_f v_f D_f$, one has $\varphi_{01} \in (0, \pi/2)$ and $\varphi_{02} \in (\pi, 3\pi/2)$. That is, the left equilibrium position is below the x -axis and the right one is above the x -axis. If $\mu^2 < c_f v_f D_f$, the reverse order can be observed. An interesting phenomenon is the critical case when two equilibrium positions happen to be on the horizontal plane, i.e., $\varphi_{01} = \pi/2$ and $\varphi_{02} = -\pi/2$, if $\mu^2 = c_f v_f D_f$. Substituting the original system parameters into this equation, one arrives at

$$\rho_c A g = \frac{1}{2} \rho_f D_c C_L V_r^2 \equiv |F_L|. \quad (38)$$

This indicates that the weight of cable of unit length is just balanced by the lift of fluid flow on the cable segment. As a consequent result, the tension in cable is balanced by the fluid drag only. In this case, the radial stretch of cable reached its minimum $8v_f D_f / \pi^5$. Obviously, this case happens only when $c_f > 0$ and $v_f > 0$ since D_f is proportional to v_f , and $\mu > 0$. Hence, the conditions of $C_L > 0$ and $V_f > 0$ should hold true. That is, the cable must be subjected to the transverse fluid flow that produces enough fluid lift.

When the cable is travelling in x direction, a more detailed form of equation (33b) reads

$$[\mu^2 - m(v_f D_f + \pi \sigma_2 \sin^2 \varphi_0)] \sin \varphi_0 - (D_f v_f + n \pi \sigma_2 \sin^2 \varphi_0) \cos \varphi_0 = 0. \quad (39)$$

By means of $\theta = \sin^2 \varphi_0$, equation (39) can be transformed to

$$a_0 \theta^3 + a_1 \theta^2 + a_2 \theta + a_3 = 0, \quad (40)$$

where

$$\begin{aligned}
 a_0 &= \pi^2 \sigma_2^2 (m^2 + n^2) \geq 0, \quad a_1 = \pi \sigma_2 [2v_f D_f (m^2 + n) - (2m\mu^2 + \pi \sigma_2 n^2)], \\
 a_2 &= (\mu^2 - mv_f D_f)^2 + v_f^2 D_f^2 - 2\pi n \sigma_2 v_f D_f, \quad a_3 = -v_f^2 D_f^2 < 0.
 \end{aligned}
 \tag{41}$$

It can be proved, through a lengthy algebraic manipulation on MAPLE, that equation (40) has only one positive real root $\theta_1 \in [0, 1]$, which corresponds to two actual roots and two pseudo-roots of equation (39). With the help of equation (39), the two pseudo-roots can be removed and a pair of rotation angles of equilibrium position is determined as follows:

$$\begin{aligned}
 \varphi_{01} &= \arccos \frac{\mu^2 - m(v_f D_f + \pi \sigma_2 \theta_1)}{\sqrt{[\mu^2 - m(v_f D_f + \pi \sigma_2 \theta_1)]^2 + (D_f v_f + n \pi \sigma_2 \theta_1)^2}} \in (0, \pi), \\
 \varphi_{02} &= \varphi_{01} + \pi \in (\pi, 2\pi).
 \end{aligned}
 \tag{42}$$

Then, equation (33a) gives the corresponding solutions of radial stretch.

5.2. STABILITY ANALYSIS

In order to analyze the stability of equilibrium positions, one should study the linear perturbation in equation (16) at (φ_{0i}, ξ_{0i}) , $i = 1, 2$. To simplify this procedure, recall the approximate solution (ξ, φ) given by equation (29) near the equilibrium position. Because $Q_2 > 0$, (ξ, φ) possesses the same stability property as $\hat{\varphi}$ governed by equation (31). Consider the perturbed equation of equation (31) at a rotation angle φ_{0i} of equilibrium position

$$\frac{d^2 \Delta \hat{\varphi}}{d\tau^2} + D_f \frac{d \Delta \hat{\varphi}}{d\tau} + \left[\left(Q_3 + \frac{\partial Q_4}{\partial \varphi_{0i}} \right) \sin \varphi_{0i} + \left(Q_4 - \frac{\partial Q_3}{\partial \varphi_{0i}} \right) \cos \varphi_{0i} \right] \Delta \hat{\varphi} = 0. \tag{43}$$

As $D_f > 0$, equation (43) is asymptotically stable if and only the following inequality holds true:

$$\left(Q_3 + \frac{\partial Q_4}{\partial \varphi_{0i}} \right) \sin \varphi_{0i} + \left(Q_4 - \frac{\partial Q_3}{\partial \varphi_{0i}} \right) \cos \varphi_{0i} > 0. \tag{44}$$

When the cable is not travelling, equation (44) can be simplified as

$$\frac{dF(\varphi_{0i})}{d\tau} = \delta_1 [(\mu^2 - c_f v_f D_f) \cos \varphi_{0i} + v_f D_f \sin \varphi_{0i}] > 0. \tag{45}$$

Substituting equation (36) into equation (45) gives

$$\frac{dF(\varphi_{01})}{d\tau} = \frac{\delta_1}{\sqrt{(\mu^2 - c_f v_f D_f)^2 + (v_f D_f)^2}} > 0, \tag{46a}$$

$$\frac{dF(\varphi_{02})}{d\tau} = \frac{\delta_1}{\sqrt{(\mu^2 - c_f v_f D_f)^2 + (v_f D_f)^2}} < 0. \tag{46b}$$

Hence, the left equilibrium position is always asymptotically stable and the right equilibrium position is unstable when the fluid flows from the right to the left. It is easy to see that the right equilibrium position is a saddle point.

In the case of travelling cable, it seems impossible to derive an analytical stability criterion like equation (46) for the equilibrium positions. However, the tuition and a great number of numerical examples support the similar assertion. That is, the left equilibrium position is asymptotically stable.

6. CASE STUDIES

6.1. ACCURACY OF APPROXIMATE SOLUTION

To check the accuracy of approximate solution (29) determined by equation (31) with a small parameter μ , a great number of numerical comparisons were made between the

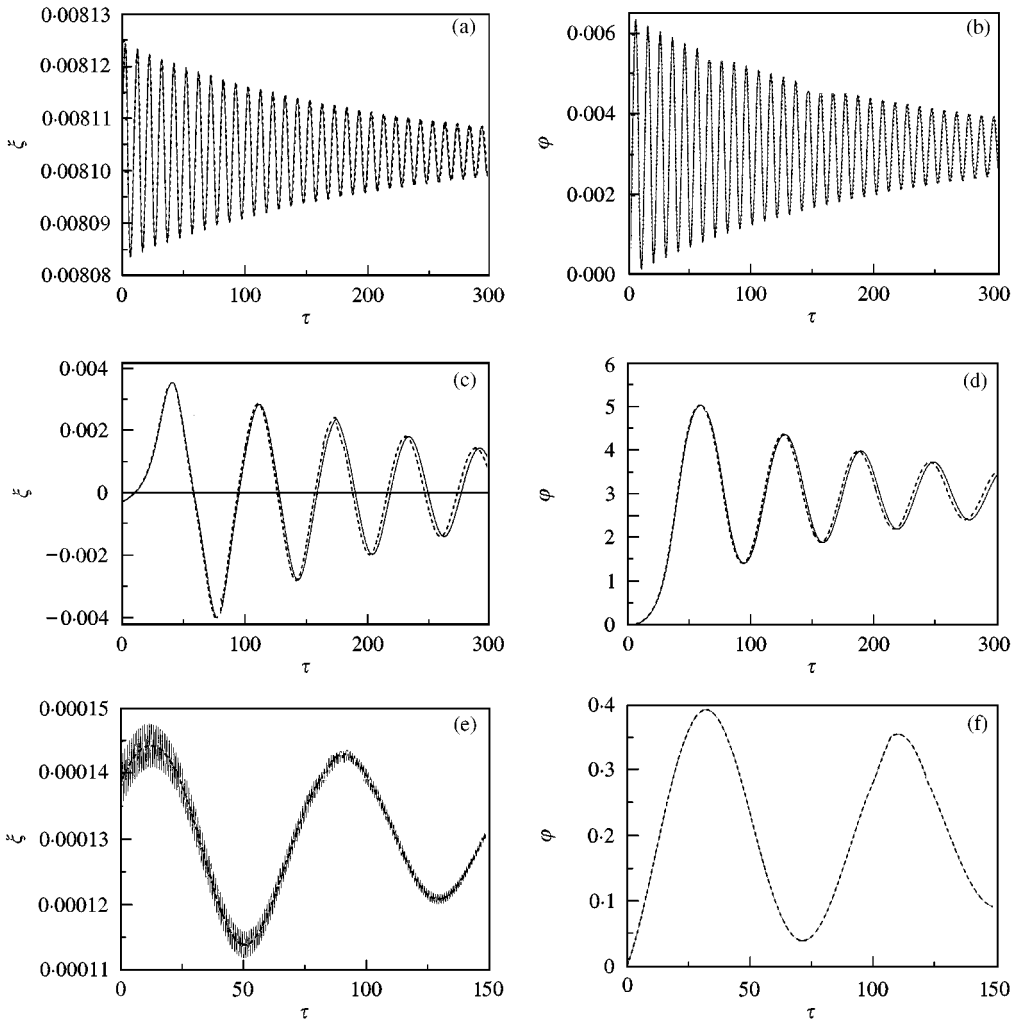


Figure 5. Comparison between solutions of equations (16) and (31) ($d = 0.1, c_f = 0.5, v_f = 0.1, D_f = 0.1$). (a) Stretch ($\mu = 0.6, \lambda_0 = 100$); (b) Rotation angle ($\mu = 0.6, \lambda_0 = 100$); (c) Stretch ($\mu = 0.3, \lambda_0 = 200$); (d) Rotation angle ($\mu = 0.3, \lambda_0 = 200$); (e) Stretch ($\mu = 0.1, \lambda_0 = 10$); (f) Rotation angle ($\mu = 0.1, \lambda_0 = 10$), —, exact; - - - -, approximate.

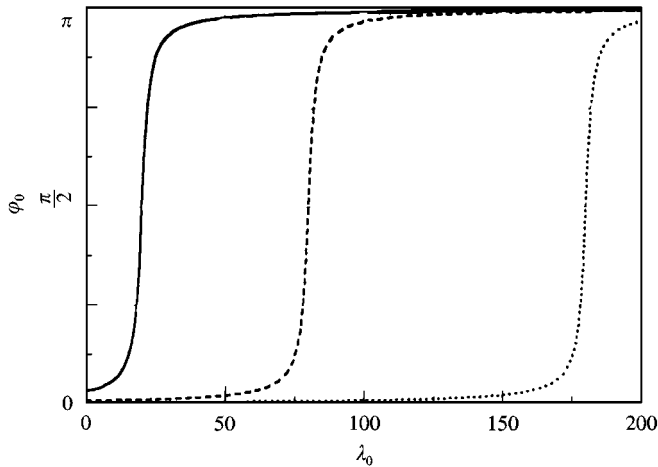


Figure 6. Rotation angle of stable equilibrium position versus relative travelling velocity for three specific values of μ ($d = 0.1$, $c_f = 0.5$, $v_f = 0.1$, $D_f = 0.1$). —, $\mu = 0.1$; - - - - , $\mu = 0.2$; ····, $\mu = 0.3$.

approximate solution and the numerical solution of equation (16), which is referred to as “exact solution” for short. All the numerical examples showed very good agreement between those two kinds of solutions in a wide range of parameters. For example, it is very hard to identify the difference between the exact and approximate solution shown in Figures 5(a) and 5(b) even for $\mu = 0.6$ and $\lambda_0 = 100$. Figures 5(c) and 5(d) show an identifiable, but very small difference between the exact and approximate solutions when the travelling velocity was so high that $\lim_{\tau \rightarrow +\infty} \varphi(\tau) \rightarrow 3.04$, i.e., the mid-span section of cable arrived at the top equilibrium position.

It should be pointed out that in the above two case studies, the initial state of solution (29) was set to meet the requirement of $\varphi_0(0) = 0$, $\dot{\varphi}_0(0) = 0$, $\alpha_0 = 0$, $\beta_0 = 0$, and so was the state of exact solution. As a result, the high-frequency components do not appear in the stretch and rotation of cable. To show the accuracy of approximate solution when the exact solution involves high-frequency components, Figures 5(e) and 5(f) give the comparison of exact and approximate solutions when $\varphi_0(0) = 0$, $\dot{\varphi}_0(0) = 0.01$, $\alpha_0 = 0$, $\beta_0 = 0$. In this case, the approximate stretch offers a kind of averaged slow trend, as shown in Figure 5(e), of the exact stretch, which engineers are interested in. As for the rotation angle, the approximate solution still coincides with the exact one as shown in Figure 5(f).

6.2. EFFECTS OF TRAVELLING VELOCITY AND CABLE DENSITY ON DYNAMICS

In this study, the system parameters were set at $d = 0.1$, $c_f = 0.5$, $D_f = 0.1$, $v_f = 0.1$, while parameters μ and λ_0 were taken as the two changeable parameters. As v_f was fixed, the change of λ_0 represents only the variation of travelling velocity c . In addition, the change of μ can be understood as the variation in cable density of ρ_c only, because D_f and v_f appear in the form of product in equation (31) so that the total density of cable system ρ disappears.

To gain an insight into the cable dynamics, the rotation angles of equilibrium position of cable were computed according to equations (40) and (42) first. Figure 6 shows the rotation angle of asymptotically stable equilibrium position of cable with increase of travelling velocity for three specific values of μ . The three curves in the similar shapes indicate that the stable equilibrium position always goes up from the bottom to the top with increase of

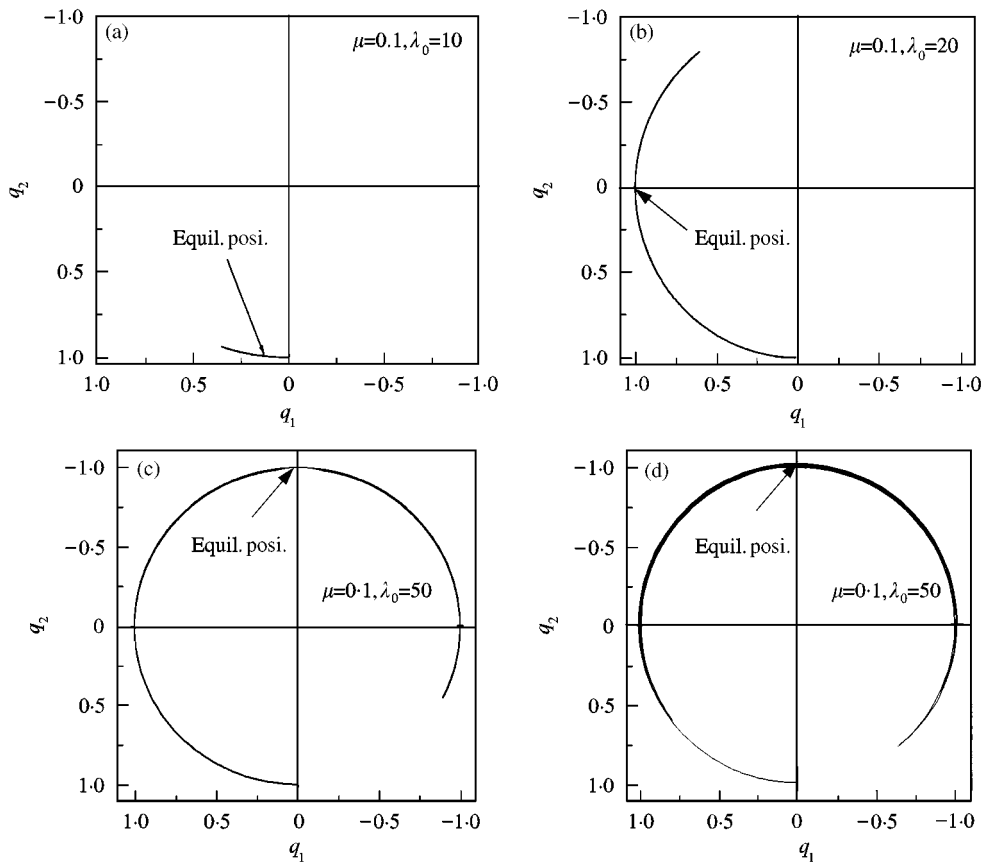


Figure 7. Motions of mid-span section of cable at different travelling velocities ($\mu = 0.1$, $d = 0.1$, $c_f = 0.5$, $v_f = 0.1$, $D_f = 0.1$). (a) $\lambda_0 = 10$; (b) $\lambda_0 = 20$; (c) $\lambda_0 = 50$; (d) $\lambda_0 = 200$.

travelling velocity, and the transition from the bottom to the top is very sudden at a specific travelling velocity. Moreover, the increase of parameter μ , i.e., the density of cable, can greatly increase the above transition velocity.

Figure 7 shows the cable dynamics in the case of $\mu = 0.1$. When the travelling velocity was low, e.g., $\lambda_0 = 10$, the cable had a few swings around the low-equilibrium position first and then returned to it as shown in Figure 7(a). With increase of travelling velocity, the stable equilibrium position of cable moved up and reached the plane of xoy as shown in Figure 7(b) when $\lambda_0 = 20$. To well understand this phenomenon, the global phase flow of equation (31) in this case is shown in Figure 8, where the equilibrium position at $\varphi_0 \approx 1.571 \approx \pi/2$ is an asymptotically stable focus and the equilibrium position at $\varphi_0 \approx 4.713 \approx 3\pi/2$ is an unstable saddle. If the travelling velocity is further increased, the cable would swing a few circles around the x -axis as shown in Figure 7(c) when $\lambda_0 = 100$ or even repeated many times as shown in Figure 7(d) when $\lambda_0 = 200$, and finally returned to the stable equilibrium position at the top. This phenomenon may cause troubles in marine engineering when an underwater cable is laid.

According to Figure 6, the cable density can greatly drop the equilibrium position and may reduce the possibility of large swing. Thus, the cable dynamics at $\mu = 0.3$ was studied. Figure 9(a) shows the motion of mid-span section of cable when $\lambda_0 = 50$. In this case, the large density prevented the cable from getting up by nature, and made the cable swing with

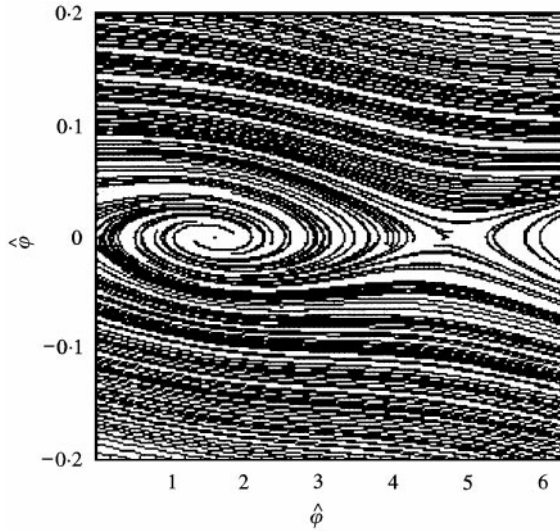


Figure 8. Global phase flow of equation (31). ($\mu = 0.1, \lambda_0 = 20, d = 0.1, c_f = 0.5, v_f = 0.1, D_f = 0.1$).

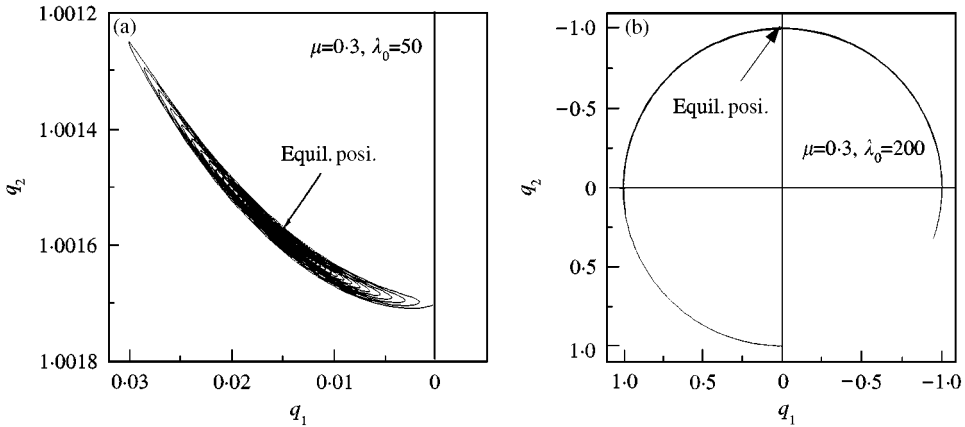


Figure 9. Motions of mid-span section of cable at different travelling velocities ($\mu = 0.3, d = 0.1, c_f = 0.5, v_f = 0.1, D_f = 0.1$) (a) $\lambda_0 = 50$; (b) $\lambda_0 = 200$.

very small amplitude and return to the stable equilibrium position at the bottom. When $\lambda_0 = 200$, the stable equilibrium position of cable moved to the top as shown in Figure 9(b). Hence, the mid-span section of cable would undergo a couple of swings around the x -axis and settled down to the top equilibrium position at last.

7. CONCLUDING REMARKS

The motion of a suspended travelling cable subjected to transverse fluid flow can be approximately described by a two-dimensional autonomous system when the sag-to-span ratio is small and the Young's module of cable is large enough. In this case, the mid-span section of cable moves and vibrates like a spring pendulum. The cable has two equilibrium configurations. One is asymptotically stable and the other is unstable. With increase of

travelling velocity, the stable equilibrium position of mid-span section of cable can move up from the bottom to the top of a circle. In addition, the cable has neither the Hopf bifurcation nor the chaotic motions.

The numerical computations showed that the cable had swings of small amplitude around the equilibrium position when the travelling velocity was relatively low. With the increase of travelling velocity, the cable might exhibit repeated swings of large amplitude around the axis through two eyelets. As a result, the travelling velocity should be limited when the underwater cable is laid so as to avoid any harmful or dangerous rotations.

If the fluid flow is not perpendicular to the vertical plane, the dynamic equations of cable will become much more complicated due to the components of fluid drag and lift in x direction. Some basic assumptions in section 2 may not hold true in this case. Thus, the dynamics of a suspended travelling cable subjected to the fluid flow in arbitrary direction is still an open problem.

ACKNOWLEDGMENTS

This work was supported in part by the “333 Talent Project” of Jiangsu Provincial Government, the People’s Republic of China.

REFERENCES

1. Y. CHOO and M. J. CASARELLA 1973 *Journal of Hydraulics* **7**, 137–144. A survey of analytical methods for dynamic simulation of cable-body systems.
2. S. NAIR and G. HEGEMIER 1979 *Journal of Hydraulics* **13**, 20–27. Stability of faired underwater towing cables.
3. C. Y. HUNG and S. NAIR 1984 *AIAA Journal* **22**, 1786–1790. Planar towing and hydroelastic stability of faired underwater cables.
4. V. J. PAPAZOGLU, S. A. MAVRAKO and M. S. TRIANTAFYLLOU 1990 *Journal of Sound and Vibration* **140**, 103–115. Nonlinear cable response and model testing in water.
5. D. VASSALOS and S. HUANG 1996 *Computers and Structures* **58**, 557–562. Dynamics of small-sagged taut-slack marine cable.
6. S. A. MAVRAKOS and J. CHATJIGEORGIOU 1997 *Computers and Structures* **64**, 819–835. Dynamic behavior of deep water mooring lines with submerged buoys.
7. W. K. CHANG, V. N. PILIPCHUK and R. A. IBRAHIM 1997 *Nonlinear Dynamics* **14**, 377–406. Fluid flow-induced nonlinear vibration of suspended cables.
8. N. PERKINS and C. D. JR MOTE 1987 *Journal of Sound and Vibration* **114**, 325–340. Three-dimensional vibration of travelling elastic cables.
9. V. N. PILIPCHUK 1986 *Soviet Applied Mechanics* **22**, 162–168. Method of investigating nonlinear dynamics problems of rectangular plates with initial imperfections.
10. J. KEVORKIAN and J. D. COLE 1981 *Perturbation Methods in Applied Mathematics*, 115–119. New York: Springer.